Modeling Cage-to-Cage Dynamics of Adsorbates at Arbitrary Loadings with Dynamically Corrected Transition-State Theory

Canan Tunca and David M. Ford*

Department of Chemical Engineering, Texas A&M University, College Station, Texas 77843-3122

Received: June 24, 2002; In Final Form: August 21, 2002

Transition state theory (TST) formalisms have allowed researchers to extend the time and length scales accessible to the modeling of diffusion in microporous materials. In a previous paper (Tunca, C.; Ford, D. M. *J. Chem. Phys.* **1999**, *111*, 2751), we used multidimensional TST to obtain the escape rate of adsorbate molecules from an α cage in zeolite ZK4 as a function of loading. A physically reasonable approximation was applied to make the TST partition functions tractable, and they were evaluated with a nested Widom insertion scheme. However, that study was limited to the case of empty neighboring cages and nondynamically corrected rate constants. This paper extends the work in several ways. First, we consider the effects of adsorbate occupancy in the neighboring cages. Our results show that the TST escape rates increase with loading in the original cage but show nonmonotonic behavior with respect to loading in the destination cage. Furthermore, we employ an expanded ensemble method (EEM) to obtain the partition functions, thus avoiding the limitations associated with the Widom insertions used previously. Even at high cage loadings, the results have small statistical errors due to the use of the EEM. Finally, we calculate and present dynamical corrections to the rate constants. The dynamical corrections are rather modest in magnitude for this model system, typically representing changes of about 10% relative to the TST values.

I. Introduction

Molecular dynamics (MD) simulations have been successfully used to model the transport of adsorbed molecules in nanoporous materials. However, current computational capabilities limit the systems to which MD can be applied. Transition state theory (TST), in combination with stochastic dynamics, provides a powerful tool for extending the time and length scales over which transport coefficients can be predicted; refs 1 and 2 provide more detailed discussion and review.

One major challenge for TST is the prediction of the concentration dependence of diffusion rates in nanoporous materials. This is generally a difficult problem because the TST partition functions increase in dimensionality with the number of particles involved in a hopping event, and just defining the limits on the integrals may quickly become unfeasible.[3] The development of practical and accurate approximations is therefore necessary, but the type of approximation that will be adequate depends strongly on the nature of the particular system being modeled.[3−6] A recent example is the use of mean-field corrections to treat many-body effects in benzene−NaX systems, where the sorbate−sorbate interactions are perturbations on the very strong sorbate-host interactions.[2]

Tunca and Ford[1] have addressed a different situation, where adsorption is not highly localized and the sorbate−sorbate interactions are comparable in strength to the sorbate-host interactions. Such a situation can be realized within the cages of highly siliceous zeolites or within the nanopores of carbon materials. Tunca and Ford modeled the particular case of methane and xenon escaping from a loaded α cage in aluminum-free ZK4 into empty neighboring cages. They developed a physically reasonable "low-dimensional approximation" to make the many-dimensional TST partition functions tractable, and they solved the integrals with a method introduced by Kaminsky[7] that employs Widom[8] test insertions.

Although the nested approach of Kaminsky avoided problems associated with the inefficiencies of inserting many particles, the single-particle Widom insertions still suffered from statistical inefficiencies at higher loadings. Recently, expanded ensemble methods (EEMs) have been developed and used successfully to calculate the chemical potentials of dense fluids and polymers.[9−17] The basic idea is to have one particle in the system that couples to the rest of the particles in incremental stages, with sampling of these stages included in the Monte Carlo walk. Although the intermediate configurations of the test particle do not contribute directly to the statistics, they provide a smooth pathway between a full particle and a ghost particle. Furthermore, transitions along this pathway are greatly enhanced with the use of bias functions that equalize the occupation probabilities of the stages. Improvements of many orders of magnitude in statistical quality can be achieved with EEM in chemical potential calculations for dense and complex fluids.

Probably the most significant assumption in TST rate calculations is that of thermalization in the destination state after barrier crossing.[5,18] This assumption is not always accurate. The diffusing particle may undergo a dynamical recrossing, where it quickly bounces back and thermalizes in the original state, or a dynamical multistate crossing, where it quickly passes through the first destination state and thermalizes in some different state. Both effects will cause the true rate constant to deviate from the TST value. Dynamical corrections for such effects may be systematically obtained from relatively short MD simulations, originated on the TST dividing surface.[5] An additional benefit of dynamical corrections is that they will naturally correct for any errors or approximations associated

* To whom correspondence should be addressed. Phone (979) 862-4850. Fax (979) 845-6446. E-mail: D-Ford@chennov2.tamu.edu.

10.1021/jp026375j CCC: $22.00
Published on Web 09/28/2002

with the TST dividing surface. Since one of the main concepts of this paper is an approximate construction of the TST surface, dynamical corrections are an important issue.

There are three main goals of this work. One goal is to extend our study of TST escape rates to cases where neighboring cages are occupied; this is of course necessary for the development of realistic stochastic models of diffusion. We will meet this goal by calculating the rate of adsorbate hopping between two adjacent cages, each at an arbitrary loading. The second goal is to incorporate an EEM into Kaminsky's scheme for evaluating multidimensional partition functions of fluids in pores. To our knowledge, this work is the first to use an EEM to evaluate such partition functions. Our final goal is to obtain dynamical corrections to our TST rate constants and evaluate their importance. In section II, we present the necessary background and develop our extended theory. In section III, the model systems and calculational details are described. The results are presented and discussed in section IV. Conclusions are outlined in section V.

II. Theory

A. Background. The classical TST rate expression for a system with F degrees of freedom is given as follows.[4] For two adjacent local potential energy minima, denoted by i and j, the average transition rate from i to j (in units of inverse time) is given by

$$k_{i\rightarrow j}^{\mathrm{TST}} = (2\pi\beta)^{-1/2}\frac{\int_S \mathrm{d}y_1\ldots\mathrm{d}y_F \mathrm{e}^{-\beta U}}{\int_V \mathrm{d}y_1\ldots\mathrm{d}y_F \mathrm{e}^{-\beta U}} \tag{1}$$

where $\beta = 1/k_{\mathrm{B}}T$ with T the temperature and k_{B} the Boltzmann constant, S is the hypersurface connecting minimum i with minimum j, V is the hypervolume associated with minimum i, y_k is the mass-weighted coordinate for the degree of freedom k, and U is the potential energy of the system. The denominator of eq 1 is an F-dimensional integral with the system constrained to hypervolume V. The numerator of eq 1 is an $(F-1)$-dimensional integral with the system constrained to the hypersurface S. For a single spherical molecule in a rigid zeolite matrix, there are three degrees of freedom, so the numerator will be two-dimensional and the denominator will be three-dimensional.

B. Low-Dimensional (LD) Approximation. Equation 1 is rigorous, but not always useful in practice. As mentioned above, for large F it is difficult to even define the limits on the integrals, much less calculate them. Tunca and Ford[1] developed a useful approximate expression for the case of spherical molecules escaping from a loaded cage to neighboring empty cages. Here we extend the derivation of that "low-dimensional" (LD) approximation to include arbitrary loading in the neighboring cages. More specifically, we consider the rate of transition of molecules from one cage (A) to a single neighboring cage (B), as a function of loading in both A and B. As will be discussed later, we believe that such a "pairwise" consideration of cages is justified. Furthermore, we expect that any errors in our approximate LD construction of the TST dividing surface will be easily overcome through the use of dynamical correction factors.

First, we assume that the (three-dimensional) volume associated with each cage, and the (two-dimensional) surface which joins the two cages, may be defined independently of the specific configuration or loading of any guest molecules. This information might be obtained through geometric considerations, or through calculations using a single spherical adsorbate probe molecule.[1,19] Next, we consider a system with N spherical molecules distributed between the two cages A and B. In particular, we consider the state where N_A molecules are in cage A, and $N_B = N - N_A$ molecules are in the neighboring cage B. Within the LD approximation, the transition rate from this state to the state where one molecule has moved from A to B (i.e., the state where $N_A - 1$ molecules are in A and $N_B + 1$ molecules are in B) is given as

$$k_{\{N_A,N_B\}\rightarrow\{N_A-1,N_B+1\}}^{\mathrm{TST}} = (2\pi m\beta)^{-1/2} \frac{N_A\int_{S_{AB}}\int_{V_A}\ldots\int_{V_A}\int_{V_B}\ldots\int_{V_B}\mathrm{d}\mathbf{r}_{1A}^{\{2\}}\,\mathrm{d}\mathbf{r}_{2A}^{\{3\}}\ldots\mathrm{d}\mathbf{r}_{N_AA}^{\{3\}}\,\mathrm{d}\mathbf{r}_{1B}^{\{3\}}\ldots\mathrm{d}\mathbf{r}_{N_BB}^{\{3\}}\,\mathrm{e}^{-\beta U}}{\int_{V_A}\ldots\int_{V_A}\int_{V_B}\ldots\int_{V_B}\mathrm{d}\mathbf{r}_{1A}^{\{3\}}\ldots\mathrm{d}\mathbf{r}_{N_AA}^{\{3\}}\,\mathrm{d}\mathbf{r}_{1B}^{\{3\}}\ldots\mathrm{d}\mathbf{r}_{N_BB}^{\{3\}}\,\mathrm{e}^{-\beta U}} \tag{2}$$

In eq 2, m is the mass of a molecule, S_{AB} is the two-dimensional surface joining the two cages, V_A is the three-dimensional volume of cage A, V_B is the three-dimensional volume of cage B, and $\mathbf{r}_{kK}$ is the position of the kth molecule in cage K. The notation $\{N_A,N_B\} \rightarrow \{N_A - 1,N_B + 1\}$ indicates that a molecule is leaving cage A and going to the surface S_{AB}, on its way to cage B. The superscripts on the integration variables give the dimensionality of the corresponding integrals. The integral in the numerator is over the positions of all N adsorbate molecules, with molecule 1 from cage A constrained to the surface S_{AB}, and the rest of the molecules constrained to their respective cage volumes. The integral in the denominator is also over the positions of all N adsorbate molecules, with all of them constrained to their respective cage volumes. Thus, in writing eq 2, we have approximated the true $(3N-1)$-dimensional hypersurface by the hypersurface on which one of the molecules is confined to the dividing surface S_{AB}, and the rest of the molecules are confined to their cage volume. Likewise, we have approximated the true $3N$-dimensional hypervolume by the hypervolume in which all of the molecules are confined to their cage volume. Note that, for the case of $N_B = 0$, eq 2 reduces to eq 2 from ref 1.

In writing eq 2 from eq 1, we have assumed that the intracage dynamics are always fast compared to intercage hopping events and that the potential energy barriers at the cage windows are not much perturbed by the presence of multiple molecules. Thus, the LD approximation works best for cages that are large enough to allow multiple occupancy, connected to each other by very narrow necks, and energetically "uncorrugated."[1]

Recognizing that the numerator and denominator of eq 2 represent configurational partition functions, we can rewrite the equation in more convenient notation as

$$k_{\{N_A,N_B\}\rightarrow\{N_A-1,N_B+1\}}^{\mathrm{TST}} \equiv (2\pi m\beta)^{-1/2} N_A\frac{Z_S(N_A - 1,1,N_B)}{Z_V(N_A,N_B)} \tag{3}$$

The middle index of "1" in the surface integral is simply a reminder that one molecule is constrained to the dividing surface during the integration. An analogous equation can be written for the case of a molecule leaving cage B and going to the surface S_{AB}, on its way to cage A.

$$k_{\{N_A,N_B\}\rightarrow\{N_A+1,N_B-1\}}^{\mathrm{TST}} \equiv (2\pi m\beta)^{-1/2} N_B\frac{Z_S(N_A,1,N_B - 1)}{Z_V(N_A,N_B)} \tag{4}$$

Although the LD approximation makes the problem tractable in terms of providing well-defined partition function integrals,

those integrals are still challenging to evaluate. We have previously employed[1] a method introduced by Kaminsky,[7] in which the partition functions are built up in a sequential fashion using single-particle Widom insertions. For example, the ratio of the volume integrals involving N_A and N_A-1 adsorbates in cage *A*, at constant loading of cage *B*, can be written as

$$\frac{Z_V(N_A,N_B)}{Z_V(N_A-1,N_B)} = V_A\langle e^{-\beta u_t}\rangle_{N_A-1,N_B} \tag{5}$$

where u_t is the potential energy of a single inserted test molecule and the brackets represent an average over a canonical Monte Carlo (MC) simulation. In this example, the MC simulation would consist of N_A-1 molecules sampling cage *A* and N_B molecules sampling cage *B*, and the Widom test insertions would be performed in cage *A*. An equation analogous to eq 5 can also be written for the ratio of area integrals. Given that the $N_A = 1$ integral can be determined accurately through crude MC (or some other technique), eq 5 provides an efficient stepwise route to all integrals with $N_A \geq 2$.

Although this method was used in our previous work (for $N_B = 0$), it began to suffer from statistical inefficiencies at higher loadings in *A*, as reflected in the error bars of Figures 2 and 3 of ref 1. This is a well-known phenomenon when applying Widom's technique to very dense fluids.[15] In the present work, we use a more efficient technique, expanded ensembles, to evaluate the partition function ratios.

C. Expanded Ensemble Methods (EEMs). EEMs improve the efficiency with which free energy differences (i.e., partition function ratios) are determined.[9−17] The basic idea is to employ intermediate states which connect the two end states of interest, and sample these states throughout a single simulation. The intermediate states themselves are generally not of interest, but they can greatly facilitate sampling between the two end points, especially when bias functions are employed.

For example, to determine the free energy difference between two canonical systems that differ by exactly one molecule (as in eq 5 above), one begins by writing the partition function for an expanded ensemble as[12,13,17]

$$\Omega(\lambda) = \sum_{n=0}^{M} \exp(\eta_n) Z(\lambda_n) \tag{6}$$

where λ is a parameter that represents the degree of coupling of one molecule to the rest of the system, n is an index over the possible λ states (with M the total number of such states), η is a bias function, and $Z(\lambda)$ is the configurational canonical partition function of the system in a particular λ state. The number of intermediate λ states and their characteristics can be chosen in different ways, but the two end points, $n = 0$ and $n = M$, should correspond to fully decoupled and coupled molecules.

A MC walk is then performed over the degrees of freedom of the expanded ensemble. This involves two types of moves. One is the usual displacement of molecules at a fixed value of n, and the other is the change of n at fixed coordinates of the molecules. The transition probability for either type of move is given by the Metropolis criterion for the expanded ensemble,[10] $\min\{1,\exp[\Delta(U+\eta)]\}$.

The probability of visiting a particular state λ_n during the MC walk is

$$p_n = \frac{\exp(\eta_n) Z(\lambda_n)}{\Omega} \tag{7}$$

so that the ratio of partition functions for two arbitrary states i and j is given by

$$\frac{Z(\lambda_i)}{Z(\lambda_j)} = \frac{p_i \exp(-\eta_i)}{p_j \exp(-\eta_j)} \tag{8}$$

The partition function ratio for two systems that differ by one molecule can then be calculated by simply counting the number of times that each of the two end states ($n = 0$ and $n = M$) is sampled during the MC walk. To gain the maximum benefit from the EEM, the bias factors should be optimized. Certain λ states will be naturally less favored than others, and such disparities generally cause bottlenecks in sampling that result in poor connection between the two end points. The goal is to select values of the η_n such that all λ_n states have roughly equal probabilities of occupation during the walk; the states are then smoothly and equally sampled, and statistical efficiency is high. Corrections for the biasing are present in eq 8.

Applying the EEM concept to our example of two systems which differ by one molecule in cage *A* at constant loading of cage *B* (section II.B), we find that the ratio of volume integrals can be written as

$$\frac{Z_V(N_A,N_B)}{Z_V(N_A-1,N_B)} = V_A \frac{p_M \exp(-\eta_M)}{p_0 \exp(-\eta_0)} \tag{9}$$

Here, we would perform an extended ensemble MC simulation with N_A-1 full molecules sampling cage *A* and N_B full molecules sampling cage *B*; in addition, one special "coupling" molecule would sample different states and positions within cage *A*. The ratio of probabilities of the fully coupled (M) and fully decoupled (0) states of this molecule, corrected by the applied bias factors, yields the partition function ratio. As in eq 5, the factor of V_A in eq 9 represents the ideal contribution of the N_A-th molecule to the configurational integral; even if this molecule has no interaction with the others, it contributes one factor of volume to the partition function. An equation analogous to eq 9 can be written for the ratio of area integrals. For that calculation, one molecule would be confined to the surface between cages, and the coupling molecule would still be placed in the volume of cage *A*.

D. Dynamical Corrections. It is well-known that the TST rate constant may be inaccurate due to dynamical phenomena that affect the thermalization of the system shortly after barrier crossing. Chandler[18] used a correlation-function approach to develop a dynamical correction factor to the TST rate constant for a two-state system, which Voter and Doll[5] later extended to many-state systems. The multistate approach can account for phenomena like fast multistate transitions, where states not directly connected in configuration space (i.e., states not sharing a hypersurface) can become dynamically connected through intermediates, as well as fast barrier recrossing.

In the language of our model system, the result of the multistate formalism[5] can be written as

$$k_{\{N_A,N_B\}\rightarrow\{N'_A,N'_B\}} = (k^{\mathrm{TST}}_{\{N_A,N_B\}\rightarrow}) f_d(\{N_A,N_B\}\rightarrow\{N'_A,N'_B\}) \tag{10}$$

where $k^{\mathrm{TST}}_{\{N_A,N_B\}\rightarrow}$ is the *total* TST rate of leaving state $\{N_A,N_B\}$ and $f_d(\{N_A,N_B\}\rightarrow\{N'_A,N'_B\})$ is the time-dependent dynamical correction factor connecting state $\{N_A,N_B\}$ with any particular destination state $\{N'_A,N'_B\}$.

Within the context of our low-dimensional approximation, there are two distinct regions of the hypersurface surrounding a given state $\{N_A,N_B\}$. One region is associated with a molecule

moving from cage *A* to the dividing surface, while the other is associated with a molecule moving from cage *B* to the dividing surface. This implies that $k^{TST}_{\{N_A,N_B\}\rightarrow}$ is simply the sum of the TST contributions from these two regions

$$k^{TST}_{\{N_A,N_B\}\rightarrow} = k^{TST}_{\{N_A,N_B\}\rightarrow\{N_A-1,N_B+1\}} + k^{TST}_{\{N_A,N_B\}\rightarrow\{N_A+1,N_B-1\}} \quad (11)$$

More detailed expressions for the terms on the right-hand-side of eq 11 have already been given in eqs 3 and 4. Note that, in the special case of $N_A = 0$ ($N_B = 0$), only the second (first) term on the right-hand-side of eq 11 is used.

The dynamical correction factor can be represented by[5]

$$f_d(\{N_A,N_B\}\rightarrow\{N'_A,N'_B\}) = \frac{\langle v(0)\delta(0)\theta_{\{N'_A,N'_B\}}(t)\rangle}{\frac{1}{2}\langle|v(0)|\delta(0)\rangle} \quad (12)$$

where the $\delta(0)$ function ensures that the system is located on the hypersurface bounding state $\{N_A,N_B\}$ at time zero, $v(0)$ is the velocity of the transferring molecule in the direction of the local normal to the hypersurface at time zero, and $\theta_{\{N'_A,N'_B\}}(t)$ is a switching function that takes the value of 1 if the system is in state $\{N'_A,N'_B\}$ at time t and the value of 0 otherwise. The brackets denote an ensemble average with the usual Boltzmann weighting, $\exp(-\beta H)$, where the Hamiltonian H is the sum of the kinetic and potential energies. The dynamical correction factor for any pair of states can thus be obtained from the ensemble average of a set of dynamic trajectories initiated from the hypersurface surrounding the initial state. Equation 12 can also be expressed as[19]

$$f_d(\{N_A,N_B\}\rightarrow\{N'_A,N'_B\}) = (2\pi\beta m)^{1/2}\frac{\langle v(0)\delta(0)\theta_{\{N'_A,N'_B\}}(t)\rangle}{\langle\delta(0)\rangle} \quad (13)$$

Within the LD approximation, the dynamical correlation function can also be split into two separate contributions.

$$f_d(\{N_A,N_B\}\rightarrow\{N'_A,N'_B\}) = f^{A\rightarrow}_d(\{N_A,N_B\}\rightarrow\{N'_A,N'_B\}) + f^{B\rightarrow}_d(\{N_A,N_B\}\rightarrow\{N'_A,N'_B\}) \quad (14)$$

The first contribution comes from the region of the hypersurface associated with a molecule moving from cage *A* to the dividing surface, while the second comes from the region of the hypersurface associated with a molecule moving from cage *B* to the dividing surface. They are given by the following expressions

$$f^{A\rightarrow}_d(\{N_A,N_B\}\rightarrow\{N'_A,N'_B\}) = (2\pi\beta m)^{1/2}\frac{\langle v(0)\delta_A(0)\theta_{\{N'_A,N'_B\}}(t)\rangle}{\langle\delta(0)\rangle}$$

$$f^{B\rightarrow}_d(\{N_A,N_B\}\rightarrow\{N'_A,N'_B\}) = (2\pi\beta m)^{1/2}\frac{\langle v(0)\delta_B(0)\theta_{\{N'_A,N'_B\}}(t)\rangle}{\langle\delta(0)\rangle} \quad (15)$$

and the $\delta_A(0)$ function ($\delta_B(0)$ function) ensures that the system is on the region of the hypersurface where a molecule has moved from cage *A* (cage *B*) to the dividing surface at time zero. Note that, in the $t \rightarrow 0$ limit, only the correction factors $f^{A\rightarrow}_d(\{N_A,N_B\} \rightarrow \{N_A - 1,N_B + 1\})$ and $f^{B\rightarrow}_d(\{N_A,N_B\} \rightarrow \{N_A + 1,N_B - 1\})$ are nonzero. Furthermore, eq 15 shows that, in that limit, each of these functions reduces to a normalized, Boltzmann-weighted probability factor for the region of the hypersurface associated with its destination state. Therefore, the expected TST result for each of the two immediately neighboring destination states is recovered from eq 10 as $t \rightarrow 0$.

Following previous discussion in the literature, we note that the f_d should reach a plateau[5,18] or at least a linear asymptotic limit[20−22] on a time scale that is short compared to the characteristic time for a full transition event, if our corrected TST formalism is appropriate. If such a limit is indeed observed, the linear region can be extrapolated back to $t = 0$ to yield a single value for f_d that provides a meaningful, dynamically corrected transition rate. If such a limit is not observed, then there is not an adequate separation of time scales between barrier crossings and thermal events, and a TST "independent jump" model does not apply.[5,18,20−22]

TABLE 1: Values of the Parameters Used in the Lennard-Jones Model[a]

interaction	ϵ/k_B (K)	σ (Å)
CH_4-CH_4	148.184	3.817
CH_4-O	97.426	3.460

[a] Original sources are given in ref 1.

III. Model Systems and Calculational Details

A. Zeolite and Adsorbate Models. The same model zeolite employed previously,[1] pure silica (cation-free) ZK4, was used here. Spherical methane was the model adsorbate. For this model system, we previously concluded that the rate-limiting step in methane diffusion is the hop between two neighboring α cages through the eight-membered oxygen ring. Using an atomic-level model of the ZK4 and a single methane probe, we mapped out the relevant volume of an α cage and the surface joining two neighboring cages, using the voxel method of June et al.[19] Those volume and surface data will be used here; the reader is referred to ref 1 for details.

Our zeolite model consisted of a full unit cell of ZK4, which had eight α cages and an edge length of 24.6 Å. Two directly neighboring cages within this model, denoted as *A* and *B*, were used for the calculations. Periodic boundary conditions were employed when calculating the adsorbate−zeolite interactions. However, they were turned off for the adsorbate−adsorbate interactions, because we wanted to model a single, isolated pair of occupied cages.

One small difference between the present and previous results should be noted. In the previous work,[1] we presented transition rates from one α cage to any of the six empty neighboring cages. In this paper, we are considering only the jump to one specific neighboring cage, *B*. Therefore, the values for the transition rates to an empty *B* cage reported here are systematically lower (by a factor of 6) than the escape rates given in the previous paper.

B. Potentials. Since the silicon atoms are shielded by oxygen atoms in the zeolite framework, only the oxygen atoms were taken into account in the calculation of potential energy. The zeolite lattice was assumed to be rigid. The methane molecules were taken as spherical. The 12−6 Lennard-Jones potential was used to calculate methane−methane and methane−oxygen interactions.

$$u_{ij}(r) = 4\epsilon_{ij}\left[\left(\frac{\sigma_{ij}}{r}\right)^{12} - \left(\frac{\sigma_{ij}}{r}\right)^{6}\right], \quad r \le r_{cut}$$
$$= 0, \quad r > r_{cut} \quad (16)$$

The potential parameters are listed in Table 1. The cutoff was taken to be $r_{cut} = 2.5\sigma_{ij}$.

C. Evaluation of Integrals. The nested scheme indicated by eq 9 was used to evaluate the TST integrals, with the area and volume integrals determined separately. Loadings of up to 12 molecules/cage were considered in both *A* and *B*. For notational convenience, the surface and volume integrals can be thought of as elements in a matrix. The volume integrals are represented by $Z_V(N_A,N_B)$, the surface integrals for a molecule moving from *A* to *B* are represented by $Z_S(N_A - 1,1,N_B)$, and the surface integrals for a molecule moving from *B* to *A* are represented by $Z_S(N_A,1,N_B - 1)$. Due to the fact that the *A* and *B* cages are structurally equivalent, there is a great deal of symmetry in the problem that reduces the computational requirements.

For the volume integrals, the symmetry relationship is $Z_V(N_A,N_B) = Z_V(N_B,N_A)$. Two starting points, $Z_V(1,0)$ and $Z_V(1,1)$, were calculated using crude MC integration. From the $Z_V(1,0)$ point, we calculated the volume integrals for the rest of the column $Z_V(N_A,0)$, up to $N_A = 12$, by repeated application of eq 9. Due to symmetry, the row $Z_V(0,N_B)$ was then also known. This process was repeated from the $Z_V(1,1)$ point for the $Z_V(N_A,1)$ column, yielding the row $Z_V(1,N_B)$ by symmetry. Starting from the now-known element $Z_V(1,2)$, we then generated the rest of the $Z_V(N_A,2)$ column via eq 9, and obtained the row $Z_V(2,N_B)$ by symmetry. We continued in this fashion, calculating parts of columns and generating corresponding parts of rows by symmetry, until we obtained all the elements of the 0 by 12 Z_V matrix. Thus, it was sufficient to explicitly calculate only those volume integrals on and below the matrix diagonal.

For the area integrals, the symmetry relationship is $Z_S(N_A - 1,1,N_B) = Z_S(N_B,1,N_A - 1)$. The area matrix was obtained in a similar way to that described above for the volume integrals, with a few small differences. Only one starting point, $Z_S(0,1,0)$, was obtained by crude MC integration. The remainder of the column $Z_S(N_A - 1,1,0)$ was then calculated using eq 9, up to $N_A = 13$. By symmetry, this also yielded the row $Z_S(0,1,N_B)$ up to $N_B = 12$. The now-known $Z_S(0,1,1)$ was then used as the starting point for calculation of the rest of the column $Z_S(N_A - 1,1,1)$ up to $N_A = 13$, via eq 9; this also yielded the row $Z_S(1,1,N_B)$ up to $N_B = 12$ by symmetry. Again, we continued in this fashion until the area integral matrix was complete. For the area matrix, it was sufficient to explicitly calculate only those elements below the matrix diagonal.

For the area integrals, one molecule was confined to the surface and the remaining ones were confined to their respective α cage volume. For the volume integrals, all of the penetrants were confined in their respective α cage volume. Since our direct calculations were always based on changes in loading of the *A* cage, the "coupled particle" in the EEM was always constrained to the *A* cage. The constraint of a molecule to a volume (surface) was accomplished by rejecting MC moves that attempted to place this molecule outside that volume (surface). The corresponding TST rate constants were then calculated using eqs 3 and 4.

The potential parameters for the intermediate states of the coupled methane particle were taken from Kaminsky's paper.[13]

$$\sigma^{(n)} = \sigma(n/M)^{1/4} \qquad \text{for } 1 \le n \le (M-1)$$

$$\epsilon^{(n)} = \epsilon(n/M)^{1/3} \qquad \text{for } 1 \le n \le (M-1) \qquad (17)$$

The total number of states *M* was taken as 8. Lorentz−Berthelot mixing rules[23] were used for the interactions between full and intermediate methane.

The procedure given by Wilding and Müller[12] was employed to determine optimum values for the bias factors η_n. First, an estimate of the probability of each state was obtained, using a short MC simulation of 100000 steps with all bias factors set to zero. Those probabilities were plugged into the following equation to get an initial estimate of the bias factor for each *n*.

$$\eta'_n = \eta_n - \ln p(\lambda_n) \qquad (18)$$

Another short MC simulation was then performed with the updated bias factors to obtain new probabilities. This procedure was repeated until every state had roughly equal probability of being visited; two iterations were usually sufficient to accomplish this. The resulting set of bias factors was then employed in four different long runs (10^7 MC steps) initiated from different starting states, to obtain the final probabilities for $n = 0$ and $n = 8$. Those results were used to calculate the ratio of partition functions, via eq 8.

D. Calculation of Dynamical Corrections. As discussed in section II.D, there are two important, distinct regions of the hypersurface surrounding state $\{N_A,N_B\}$; the first involves a molecule moving from cage *A* to the dividing surface shared with cage *B*, and the second involves a molecule moving from cage *B* to that dividing surface. The contribution of each region to $f_d(\{N_A,N_B\}\rightarrow\{N'_A,N'_B\})$ must be investigated. Each contribution has two important parts: (1) a normalized, Boltzmann-weighted probability associated with being on that region of the hypersurface, and (2) a dynamic contribution associated with moving from that region to a particular destination state $\{N'_A,N'_B\}$ at a later time *t*.

The probability associated with being on one region of the hypersurface is simply the ratio of the surface intergal for that region to the sum of the surface integrals for both regions. The dynamic contribution for a region was estimated by initiating molecular dynamics (MD) trajectories from 1000 different starting configurations in that region. For example, for the *A* to *B* dynamic contribution, N_A-1 molecules were placed in *A* and N_B molecules were placed in *B*, while the remaining molecule was placed on the dividing surface between the cages; the system was then equilibrated with canonical Monte Carlo at 300K (constraining the N_A-1 molecules to cage *A*, the N_B molecules to cage *B*, and the other molecule to the dividing surface), and 1000 different snapshots from the MC walk were taken as starting points for MD. The initial velocities were assigned from the Maxwell−Boltzmann distribution at 300K and the trajectories were determined by microcanonical MD. The relative probabilities of being in different states $\{N'_A,N'_B\}$ at different times *t* were obtained from these sets of trajectories.

During the course of the MD simulations, reflectory boundary conditions were applied to keep the molecules from leaving the *A*-*B* two-cage model. This was done to keep the problem tractable, but it represents an important limitation because dynamically correlated transitions to other cages are not allowed. For example, events in which the original diffusing molecule would have failed to thermalize in either cage *A* or cage *B* will not be captured correctly. This issue deserves further study, but expanding the model to include neighboring cages would greatly increase the computational workload.

IV. Results and Discussion

Figure 1 shows the TST escape rate of methane from *A* to *B* as a function of N_A, for three values of N_B. The escape rate increases strongly with increasing N_A, covering 3 orders of magnitude. This increase in escape rate is due to the decrease of available free volume upon addition of adsorbate molecules in cage *A*. This entropic effect is apparently quite dominant over the attractive adsorbate−adsorbate interactions, which should

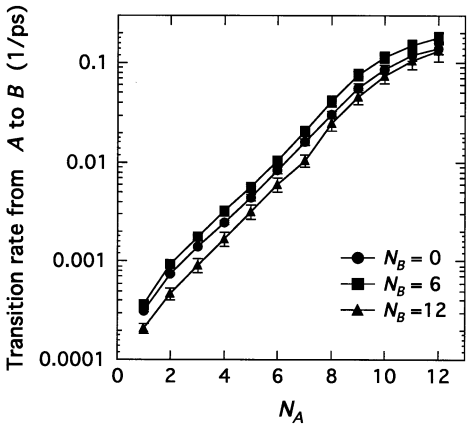

Figure 1. TST transition rate of a methane molecule from *A* to *B* as a function of N_A, for various N_B.

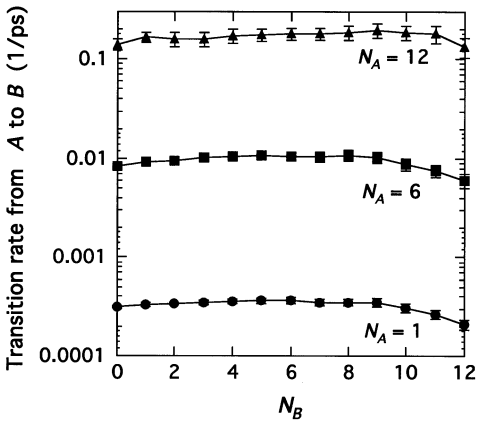

Figure 2. TST transition rate of a methane molecule from *A* to *B* as a function of N_B, for various N_A.

tend to decrease the potential energy (and the escape rate) with increased loading. Although the rates are clearly not as sensitive to N_B as they are to N_A, an interesting nonmonotonic trend is seen in Figure 1, with the $N_B = 0$ curve lying between the $N_B = 6$ and $N_B = 12$ curves. We note that the $N_B = 0$ data agree reasonably well with the methane data presented in our previous paper,[1] accounting for the fact that the present results should be systematically lower by a factor of 6 (as discussed in section III.A); the agreement is almost perfect at lower loadings, but at $N_A = 8$ the present results are smaller than the previous by about 66%.

Figure 2 provides more insight into the effects of loading in cage *B*. Initially, the escape rates increase slightly with N_B. This is likely due to attractive interactions between the molecule on the surface and the molecules in cage *B*. However, as cage *B* becomes increasingly crowded, excluded volume interactions will become more important and eventually "destabilize" the surface molecule. This trend leads to the decreases in escape rate seen at higher N_B values. The behavior observed in Figure 2 explains the nonmonotonic trend seen in Figure 1 with varying N_B. Note that the standard deviations are very small in Figures 1 and 2 even at high loadings, due to the use of the EEM.

Further insight on the transition rate behavior can be obtained by examining the area and volume TST contributions independently. Figure 3 shows the values of the area and volume integrals as functions of N_A for three values of N_B. Note that the integral values grow very quickly as either N_A or N_B increases, because each molecule in the system carries one factor of α-cage volume (1165.8 Å^3). For example, for $N_A = 1$ and $N_B = 6$, the volume integral is on the order of $V^7 \sim 10^{21}$ Å^{21}.

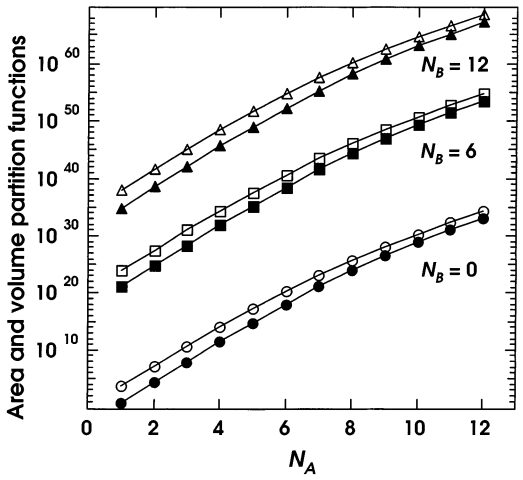

Figure 3. Values of the area integrals $Z_S(N_A - 1,1,N_B)$ and volume integrals $Z_V(N_A,N_B)$ as functions of N_A, for various N_B. The filled symbols correspond to the area integrals, and the open symbols correspond to the volume integrals. The base unit for the integrals is Angstroms.

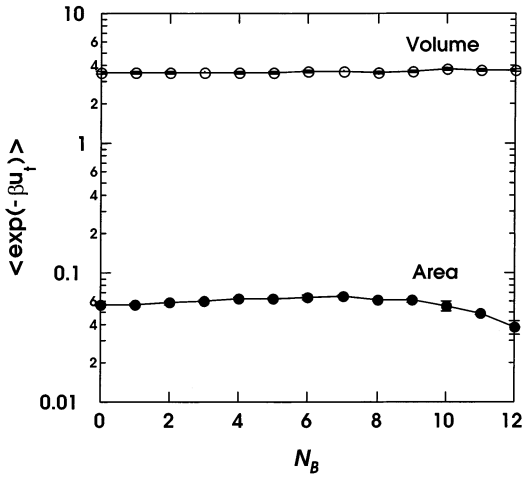

Figure 4. The average Boltzmann factor for the test insertion of a methane molecule, $\langle \exp(-\beta u_t) \rangle$, as a function of N_B. For the filled symbols (area), the test insertion was performed on the surface between cages *A* and *B*, with no molecules in cage *A*. For the open symbols (volume), the test insertion was performed in cage *A*, with no other molecules in cage *A*.

Although the general order of magnitude of the integrals is set by the total number of molecules, the important physics is captured in the Boltzmann factor integrand, $\exp(-\beta U)$, which determines the shape of the curves in Figure 3. There are three main points to note about these curves: (1) for a given N_B, the volume curves lie above the area curves, (2) the slope of each curve decreases with increasing N_A, and (3) for a given N_B, this decrease in slope is greater for the volume integral than the area integral, causing the two curves to become closer at higher N_A.

These observations can be understood in the following way. The volume integrals tend to have higher values than the corresponding area integrals for two reasons. First, the volume integrals contain an extra factor of cage length (∼ 10 Å). Second, the molecule constrained to the dividing surface in an area integral typically has a higher potential energy than its counterpart in the volume integral, so the average value of the Boltzmann factor is lower for the area integral. This energy effect becomes less important at higher loadings, as will be discussed momentarily. The slope of each curve decreases with

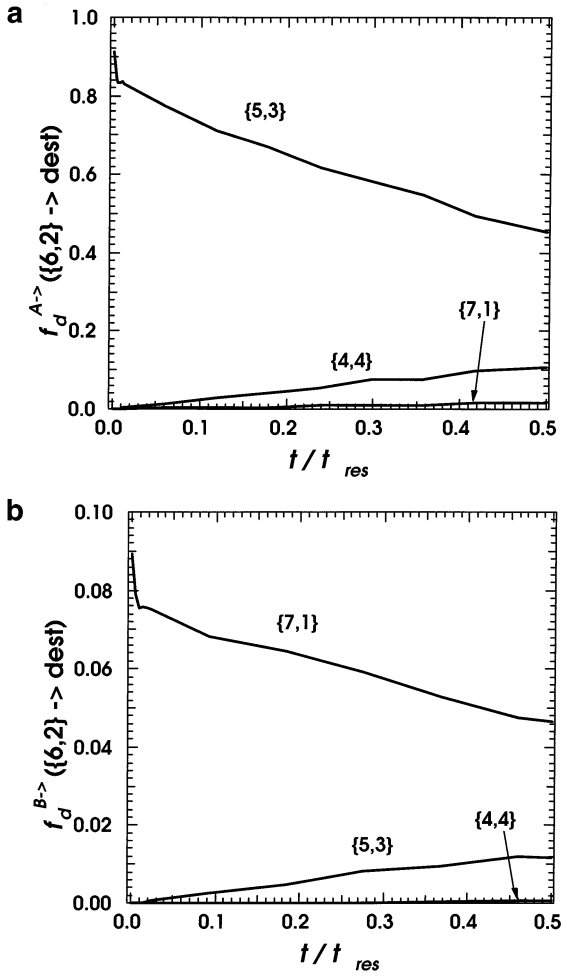

Figure 5. (a) f_d contributions for a state of {6,2}, obtained by placing five molecules in *A*, two molecules in *B*, and one molecule on the surface. Each curve represents a particular destination state of interest, as indicated by the label. (b) f_d contributions for a state of {6,2}, obtained by placing six molecules in *A*, one molecule in *B*, and one molecule on the surface. Each curve represents a particular destination state of interest, as indicated by the label.

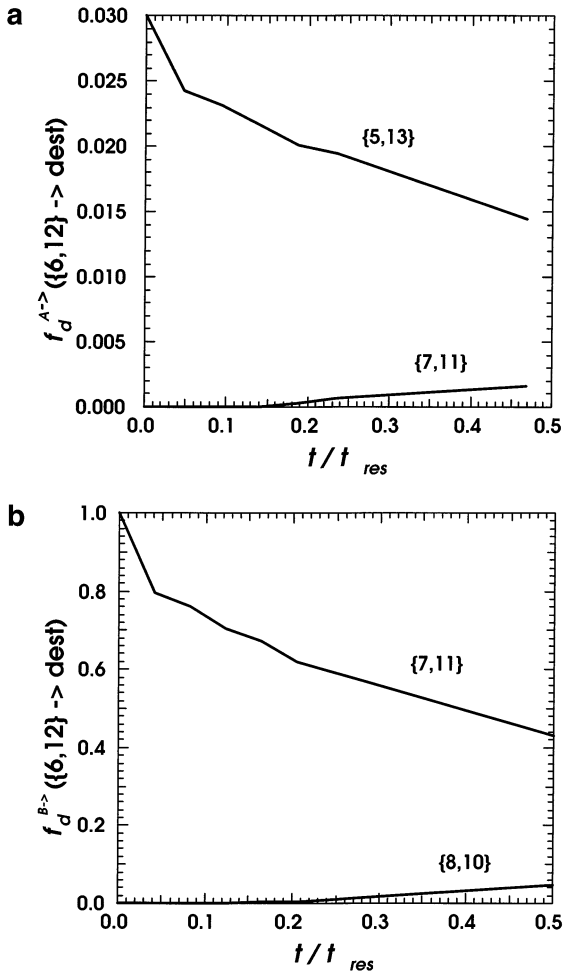

Figure 6. (a) f_d contributions for a state of {6,12}, obtained by placing 5 molecules in *A*, 12 molecules in *B*, and 1 molecule on the surface. Each curve represents a particular destination state of interest, as indicated by the label. (b) f_d contributions for a state of {6,12}, obtained by placing six molecules in *A*, 11 molecules in *B*, and one molecule on the surface. Each curve represents a particular destination state of interest, as indicated by the label.

increasing N_A because of entropic effects; there are more "overlap" configurations in the integrals at higher N_A, and the average value of the Boltzmann factor decreases. The magnitude of this decrease in slope is slightly smaller for the area integrals because one of the molecules is confined to the surface, leaving more free space in the cage. Because of this difference in slope, the area and volume curves for a given N_B approach each other at higher N_A; in principle, the curves could cross, although this was not observed for the loadings studied here. Note that this behavior leads directly to the increases in escape rate with N_A observed in Figure 1.

Another issue of interest is how strongly the molecules in one cage are affected by the presence of molecules in the neighboring cage. To study this, we employed MC simulations with an empty *A* cage and different numbers of methane molecules in cage *B*. During these MC walks, Widom test insertions of a methane molecule were performed either in the empty *A* cage, or on the surface between the two cages. The average Boltzmann factors for the inserted molecule are shown in Figure 4. Clearly, the test insertions in the volume were not affected by the loading in cage *B*, except very slightly at the highest loadings. This is very interesting because it indicates a high level of screening of inter-cage adsorbate−adsorbate interactions by the zeolite atoms, which in turn suggests that a "cage-pairwise" additivity of the free energy will be quite accurate for these model systems. The Boltzmann factors for the test insertions on the surface showed a nonmonotonic behavior similar to that seen in Figure 2. There is an initial increase due to favorable energetic interactions with the molecules in *B*, but crowding in the *B* cage eventually leads to less favorable energetic interactions and a consequent decrease in the Boltzmann factor. The results in Figure 4 suggest that focusing on one pair of cages at a time will be sufficient in this model system; other nearby cages, not directly involved in the hopping event, will not perturb that event significantly.

The dynamical correction factor $f_d^{A\rightarrow}(\{6,2\} \rightarrow \{N'_A,N'_B\})$ is shown in Figure 5a, for various destination states $\{N'_A,N'_B\}$. Note that the time axis is scaled by the inverse of the total TST transition rate, $t_{\text{res}} = (k^{\text{TST}}_{\{6,2\}\rightarrow})^{-1}$, which may be considered a mean residence time for the state; its value is 95 ps in this case. Figure 5a clearly shows that the majority of trajectories go to the neighboring {5,3} neighbor state, as might be expected, since a molecule was moved from cage *A* to the dividing surface to start the trajectories. Furthermore, there is an initial fast decay of this state, followed by a linear region that can be extrapolated back to a zero-time value of 0.835. The only other destination state with significant population on the time scale of this plot is {4,4}, which is reached via passage through the {5,3} state.

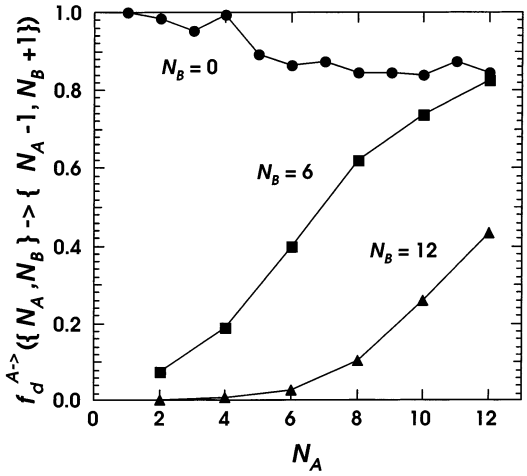

Figure 7. Dynamical correction factor for a molecule moving from *A* to *B* as a function of N_A, for various N_B.

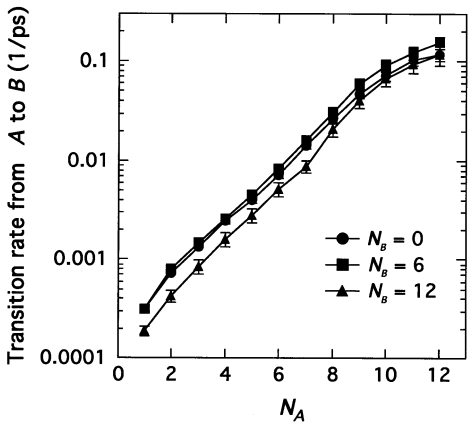

Figure 8. Dynamically corrected transition rates of a methane molecule moving from *A* to *B* as a function of N_A, for various N_B.

The contribution for the {4,4} state is linear over the same time range where the {5,3} contribution is linear; however, its linear region extrapolates back to a zero-time value of 0, indicating no contribution within the corrected TST formalism. Figure 5b shows the dynamical correction factor $f_{\mathrm{d}}^{B\rightarrow}(\{6,2\}\rightarrow\{N_A',N_B'\})$, which represents the other way that state {6,2} can decay, by a molecule moving from cage *B* to the dividing surface. The first thing to note is the much smaller scale of the ordinate, as compared to that in Figure 5a. This smaller value is due to the smaller value of the surface integral $Z_S(6,1,1)$, as compared to $Z_S(5,1,2)$. We see that the neighboring state (7,1) is the primary destination, as expected. Its f_d curve exhibits an initial fast decay, followed by a linear region that can be extrapolated back to a zero-time value of 0.075. The destination state {5,3}, accessible by passage back through the {6,2} state, starts to become important at later times, but its linear region extrapolates back to a zero-time value of 0.

Figures 6a and 6b provide similar information for the {6,-12} state. The qualitative behavior is very similar to that observed for the {6,2} state, although here the event where a molecule moves from *B* to *A* is the more heavily weighted contribution. Also, the initial fast decay regions seem to be extended relative to those in Figures 5a and 5b. This is simply because the residence time t_{res} (used to scale the time axis) is substantially smaller for the {6,12} state (5 ps). A linear asymptotic limit is still observed for the two immediately neighboring states.

All of our dynamical correction factors exhibited behavior that is qualitatively similar to that observed in Figures 5a−6b. Therefore, we can make some general conclusions regarding our system. First, a dynamically corrected TST approach appears to be meaningful, since the correction factors reach linear asymptotic limits on a time scale smaller than t_{res}. Second, the system will go to one of its two directly neighboring states; fast multistate crossings to other destinations (within the two-cage system) are not significant, as indicated by performing extrapolation of the linear regimes back to zero time. One of the neighboring states will be preferred over the other, based on the relative magnitude of its TST surface integral. Finally, the sum of the f_d values for both neighboring states tended to be around 0.9, indicating that the actual total rate of escape from a state is about 90% of the uncorrected TST value.

Figure 7 summarizes the dynamical correction factor results by presenting $f_{\mathrm{d}}^{A\rightarrow}(\{N_A, N_B\} \rightarrow \{N_A - 1, N_B + 1\})$ as a function of N_A, for several different N_B. These results were obtained from the time-dependent f_{d} data by extrapolating the linear asymptotic limits back to $t = 0$. As N_B approaches and exceeds N_A, the values of $f_{\mathrm{d}}^{A\rightarrow}$ tend to decrease because of the relatively smaller contribution of the surface integral $Z_S(N_A - 1,1,N_B)$, as compared to $Z_S(N_A,1,N_B - 1)$.

Figure 8 gives the corrected escape rates, as calculated from eq 10. Comparison with Figure 1 demonstrates that the curves have not changed qualitatively, although some small quantitative changes can be seen.

V. Conclusions

Transition rates of molecules between adjacent zeolite cages at arbitrary loadings were calculated using an approximate multidimensional TST approach. An extended ensemble method within a nested integral scheme was used to calculate the partition functions of interest. This proved to be an efficient combination, producing low standard deviations in the rate constants even at very high loadings. The rate constants increased sharply with the number of molecules in the original cage but exhibited a weaker, nonmonotonic dependence on the loading in the destination cage. These trends were explained in terms of the behavior of the individual area and volume integrals, based on entropic and energetic arguments. Furthermore, our results indicated that a "cage-pairwise" additivity of free energy is a good approximation in our model system, which should greatly simplify future analysis. The inclusion of dynamical correction factors resulted in small quantitative changes to the transition rates predicted by TST.

In future work, we will use the rate constants as input to stochastic dynamics simulations, to obtain self-diffusivity as a function of loading. Also, we will model diffusional transport across a zeolite membrane under a concentration gradient, which could be done with a dual control volume (nonequilibrium) technique[24,25] or a modified Einstein (equilibrium) method.[26]

Acknowledgment. We thank the Computational Biology & Materials Technology Department at Sandia National Laboratories for support of this work. Sandia is a multiprogram laboratory operated by Sandia Corporation, a Lockheed Martin Company, for the United States Department of Energy under Contract DE-AC04-94AL85000. Acknowledgment is made to the donors of the Petroleum Research Fund, administered by the American Chemical Society, for partial support of this research. We thank A. P. Thompson of Sandia for very helpful discussions.

References and Notes

(1) Tunca, C.; Ford, D. M. *J. Chem. Phys.* **1999**, *111*, 2751.

(2) Auerbach, S. M. *Int. Rev. Phys. Chem.* **2000**, *19*, 155.
(3) Sevick, E. M.; Bell, A. T.; Theodorou, D. N. *J. Chem. Phys.* **1993**, *98*, 3196.
(4) Vineyard, G. H. *J. Phys. Chem. Solids* **1957**, *3*, 121.
(5) Voter, A. F.; Doll, J. D. *J. Chem. Phys.* **1985**, *82*, 80.
(6) Jousse, F.; Auerbach, S. M. *J. Chem. Phys.* **1997**, *107*, 9629.
(7) Kaminsky, R. D. *Mol. Phys.* **1995**, *84*, 69.
(8) Widom, B. *J. Chem. Phys.* **1963**, *39*, 2808.
(9) Lyubartsev, A. P.; Martsinovski, A. A.; Shevkunov, S. V.; Vorontsov-Velyaminov, P. N. *J. Chem. Phys.* **1992**, *96*, 1776.
(10) Lyubartsev, A. P.; Laaksonen, A.; Vorontsov-Velyaminov, P. N. *Mol. Phys.* **1994**, *82*, 455.
(11) Attard, P. *J. Chem. Phys.* **1993**, *98*, 2225.
(12) Wilding, N. B.; Muller, M. *J. Chem. Phys.* **1994**, *101*, 4324.
(13) Kaminsky, R. D. *J. Chem. Phys.* **1994**, *101*, 4986.
(14) Escobedo, F. A.; de Pablo, J. J. *J. Chem. Phys.* **1995**, *103*, 2703.
(15) Kofke, D. A.; Cummings, P. T. *Mol. Phys.* **1997**, *92*, 973.
(16) de Pablo, J. J.; Yan, Q.; Escobedo, F. A. *Annu. Rev. Phys. Chem.* **1999**, *50*, 377.
(17) Khare, A. A.; Rutledge, G. C. *J. Chem. Phys.* **1999**, *110*, 3063.
(18) Chandler, D. *J. Chem. Phys.* **1978**, *68*, 2959.
(19) June, R. L.; Bell, A. T.; Theodorou, D. N. *J. Phys. Chem.* **1991**, *95*, 8866.
(20) Adams, J. E.; Doll, J. D. *J. Chem. Phys.* **1984**, *80*, 1681.
(21) Berne, B. J.; Borkovec, M.; Straub, J. E. *J. Phys. Chem.* **1988**, *92*, 3711.
(22) Mosell, T.; Schrimpf, G.; Hahn, C.; Brickmann, J. *J. Phys. Chem.* **1996**, *100*, 4571.
(23) Allen, M. P.; Tildesley, D. J. *Computer Simulation of Liquids*; Clarendon Press: Oxford, 1987.
(24) Pohl, P. I.; Heffelfinger, G. S.; Smith, D. M. *Mol. Phys.* **1996**, *89*, 1725.
(25) Pohl, P. I.; Heffelfinger, G. S. *J. Membr. Sci.* **1999**, *155*, 1.
(26) Skoulidas, A. I.; Sholl, D. S. *J. Phys. Chem. B* **2002**, *106*, 5058.